

Supporting Online Material

The density functional theory (DFT) calculations were carried out using the dacapo code (<http://www.fysik.dtu.dk/CAMPOS>), and the RPBE (1) generalized gradient correction (GGA) to treat exchange and correlation effect. The core electrons of all the atoms were treated with Vanderbilt ultra-soft pseudopotentials (2) and the energy cut off was 340 eV. A Chadi-Cohen grid of 6 special k -points was used together with a Fermi smearing of 0.1 eV for the sampling of the Brillouin zone. The Ru steps were modeled by using a three-layers thick slab (3) of Ru(001) and a (5x2) surface cell where two closed-packed rows were removed to form a step. The transition states were localized constraining the N-N distance and relaxing all of the other degrees of freedom including the topmost two layers of metal atoms. By varying the N-N distance, we localize the saddle point.

We consider the following elementary reaction steps in the NH_3 synthesis:



where * and X^* correspond to an empty site and an adsorbed X species, respectively. The first reaction step actually consists of two consecutive steps, N_2 adsorption and dissociation, but kinetically they can be treated as one, since the molecular adsorption step is at equilibrium, and the N_2 coverage is negligible for all of the reaction conditions of interest here.

In Table S1 we present the calculated adsorption geometries and their energies, calculated with respect to gas-phase N_2 and H_2 , for all of the intermediates according to Eq. 1. The zero-point corrected reaction energy for formation of gas-phase NH_3 is 0.55 eV.

Table S2 gives the vibrational frequencies calculated by diagonalizing the Hessian matrix. To obtain the Hessian matrix one N or H atom at a time was displaced in three different Cartesian directions around the equilibrium or saddle point. The frequencies are needed to determine vibrational partition functions that are then used to calculate entropy contributions.

$$\Delta S = k_B \ln q, \quad (2)$$

where q is the appropriate vibrational partition function given by

$$q = \prod_i \frac{1}{1 - e^{-h\omega_i/2\pi k_B T}}.$$

For the calculation of the prefactor ν in the rate equation, $k_i = \nu e^{-E_{a,i}/kT}$, we use the harmonic transition state theory:

$$\nu = \frac{k_B T}{h} \frac{q_{TS}}{q_{gas}}, \quad (3)$$

where q_{TS} and q_{gas} are the partition functions.

We have also calculated adsorption energies of different intermediates on the upper and lower steps at different coverages. From this, the interaction between the intermediates can be determined using a simple pair wise interaction model.

Geometries and adsorbate-adsorbate interactions along the step for the upper step sites, together with the H-H interaction for the lower step sites, are given in Table S3. Sites at the upper and lower step are so far apart that there is no nearest-neighbor adsorbate-adsorbate interaction between these sites. The effect of H on the terrace behind the step has been included implicitly in the interactions of adsorbates with H along the step by having adsorbed H on the terrace next to the step when calculating the energy of the high coverage states (see Table S3). Adsorbed H is the only species with an appreciable coverage on the terraces.

The thermodynamic equilibrium is established by Monte Carlo (MC) techniques applying the Metropolis algorithm (4). We use the Grand Canonical ensemble to ensure that a MC simulation reaches this equilibrium. The following events are included reaction, exchange, and adsorption/desorption.

The gas-phase is described by pressure- and temperature-dependent chemical potentials (5,6) for H_2 and NH_3 :

$$\mu_H(T, p_{H_2}) = -\frac{1}{2} k_B T \ln q_{H_2} + \frac{1}{2} k_B T \ln \frac{p_{H_2}}{p_0}, \quad (4)$$

and

$$\mu_{NH_3}(T, p_{NH_3}) = -k_B T \ln q_{NH_3} + k_B T \ln \frac{p_{NH_3}}{p_0}, \quad (5)$$

where q_{H_2} and q_{NH_3} are partition functions determined from DFT values. The reference pressure p_0 is 1 bar.

Due to the absence of nearest neighbor adsorbate-adsorbate interactions between the upper and lower step sites, we model the stepped Ru surface with two independent one-dimensional periodic lattices consisting of 50 sites. After an initial thermalization of one million MC iterations, the ensemble of configurations was sampled every thousand MC iteration. The number of samples used to achieve good statistics equals a hundred thousand.

The coverage, Θ , is determined by calculating the occurrence of a certain adsorbate whereas the conditional probability $P(A|*)$ of having one specific neighbor, A , next to an empty site $*$ is determined by calculating the joint probability, $P(A*)$, for such pairs in the ensemble of local environments obtained in the MC simulation. This joint probability is then converted to the desired conditional probability by dividing by the coverage of empty sites. Hence, the mathematical expression for the probability of the local environment, P_i , is

$$P_i = \Theta_*^{upper} P(A|*)P(B|*)\Theta_*^{lower} P(C|*)P(D|*) \quad (6)$$

where Θ_*^{upper} is the coverage of empty sites in the upper step, Θ_*^{lower} is the coverage of empty sites on the lower step, and A, B, C, D can be any of the adsorbed species H, N, NH, NH₂, NH₃.

Fig. S1 shows the coverages and conditional probabilities calculated in the MC simulation both with (interaction) and without (mean-field) the interactions between the adsorbates. Under the condition used in Fig. S1, the inclusion of interactions decreases the coverage of H atoms and empty sites whereas the coverage of NH₂ molecules increases substantially. This is also reflected in the conditional probability. In addition, Fig. S1 shows that all of the adsorbate-adsorbate interactions are needed only on the upper step, whereas on the lower step only the hydrogen interaction is important.

Figs. S2. A and B present the local environments that contribute mostly to the total rate when integrating through the reactor. Note that it is not the rate with the lowest activation energy that makes

the largest contribution to the total rate. The reason is that the probability to have the local environment associated with the lowest activation energy is very small under the synthesis conditions. So in general, a balance between the activation energy and the probability for that local environment determines which rate that gives the largest contribute to the total rate. Furthermore, Fig 2S shows that the probability of finding these environments varies substantially down the reactor. As NH_3 is produced, the coverage of N-containing species on the surface increases and the low-barrier configurations become scarcer. The activity of the catalyst is therefore considerably larger at the entrance to the reactor than at the exit.

In Fig. S3 we compare the NH_3 productivity using three different models. The basic mean field model neglects all interactions between adsorbates and includes only one local environment: N_2 dissociation on the empty surface. The mean field model includes all contributions from different local environments to the rate, but still neglects adsorbate-adsorbate interactions. This leads at least two orders of magnitude higher NH_3 productivity compared with the basic mean field model. The interaction model including different local environments and the adsorbate-adsorbate interactions gives by far the highest NH_3 productivity of all the models. The interactions and several different local environments are clearly important for the absolute accuracy of the model, but even the simplest model captures the trends quite well.

While the overall rate of ammonia synthesis is not very sensitive to the errors in the absolute adsorption energies it could depend more sensitively on the relative errors in adsorption energies of different adsorbates. To test this, we have decreased the adsorption energy of H atoms by 0.06 eV. The results are shown in the Fig. S4 where we compare the productivity calculated using the original DFT energies and the productivity obtained with a modified H adsorption energy. Clearly a small change in the relative energies is enough to give an absolute agreement between theory and experiment at all temperatures and flows.

The number of active sites of the nano-particles is determined in the following manner. First the surface energies are calculated using DFT, in the same implementation used for the calculations of the NH_3 synthesis energetics. The slabs used have at least 4 layers of Ru atoms and are between 7 and 9 Å thick. Subsequent slabs are separated by at least 11 Å of vacuum. When N Ru atoms are

exposed in each of the two sides of the slab, we use $2N$ atoms in the middle of the slab that was kept frozen in the bulk Ru positions. A Monkhorst-Pack grid of special k-points was used to sample the Brillouin zone of the system. An $8 \times 8 \times 1$ grid was used for Ru(001), scaled appropriately for the other surfaces. The surface energy is defined as $E_{surf} = (E_{tot} - N E_{bulk}) / 2A$, where N is the number of atoms in the unit cell, E_{tot} is the calculated total energy, E_{bulk} the calculated total energy per atom of hcp Ru, and A is the surface area. The factor 2 accounts for the two surfaces in the two sides of the slab. Table S4 summarizes the calculated surface energies (in J/m^2) for all of the Ru(hkl) surfaces with $h+k+l < 4$. For most of the (hkl) planes in an hcp crystal there exist two structures, labeled A and B, depending on the position of the cleavage plane.

Using the calculated surface energies, we make a Wulff construction that shows the equilibrium shape of the crystal. The construction is shown in Fig. S5. The dominant faces are (001), (100) and (101). None of the faces appearing in the Wulff construction contains B_5 sites. On the other hand, the Wulff construction is valid only for very large crystals, as it does not take into account edge effects. In the present case, the Ru particles are in the range between 1 to 5 nm, and their shape will be strongly modified by edge effects. To take that into account, we consider Ru(103), shown in Fig. S6. The two structures of Ru(103), depending on the position of the cleavage plane, are equivalent to a periodic arrangement of (001)/(101) edges (Ru(103)A), and a periodic "ladder" with alternative A- and B-type steps. We find that the later is more stable by about 0.1 eV/atom. Therefore, we remove the atoms in the edge between (001) and (101), to create a monoatomic step. The thus constructed Ru nanoparticles are similar to the one shown in Fig. 3 of the manuscript.

We define a B_5 site based on the coordination number of the Ru atoms. Such a site occurs when a step-edge atom (with coordination number 7) neighbors with another two step-edge atoms, two terrace atoms (with coordination number 9), two bulk atoms (with coordination number 12) and a lower terrace atom (with coordination number of 10). Such sites occur only in three of the six (001)/(101) edges in each side of the particle, see Fig. 3 of the manuscript. The number of active sites increases with increasing particle size, as it is roughly proportional to its diameter. As the mass of the particle is proportional to its volume, or the cube of the diameter, the active site density (sites per gram of Ru) decreases roughly as $1/d^2$, d being the diameter. For particles with an average diameter smaller than 1.94 nm, there are no active sites, as the (001)/(101) edge is less than 2 atoms long.

This is observed in the plot shown in Fig. 3 of the manuscript. In this plot, we have used the Ru loading of the catalyst (11.1 wt %) to calculate the number of active sites per gram of catalyst. To find the average number of active sites, we integrate the thus calculated number of active sites per gram of catalyst for a fixed particle size with the particle size distribution, also shown in Fig. 3 of the manuscript. The result is 9.64 $\mu\text{mol/g}$.

Transmission Electron Microscopy (TEM) images were recorded using a Philips CM200 FEG UltraTwin operated at 200kV (information limit 0.12 nm). Images were obtained on a sample of the catalyst that were reduces ex situ in H_2 at 300°C in a plug flow reactor. The sample was transferred to the microscope via a glove box in order to avoid exposure to oxygen. The Ru particle size distribution was obtained from high-angle annular darkfield Scanning TEM images that were processed using the ImagePro+ software for automatic particle identification and measurement. Approximately 1000 particles that were situated in 6 different areas on the sample were included in the Ru particle size distribution.

The preparation and the NH_3 synthesis activity measurements of the Ru catalyst has been described earlier (7). The catalyst consists of 11.1 wt% Ru supported on a magnesium aluminum spinel support with a surface area of 52 m^2/g . The NH_3 synthesis activities were determined using a plug flow reactor and a wide range of process conditions. The temperature was varied between 320 and 440 °C, the pressure between 1 and 100 bar, and the flow between 40 and 267 ml/min (STP). To avoid being limited by the equilibrium, the measurement was performed within 0 to 20% conversion of the equilibrium.

FIG 1

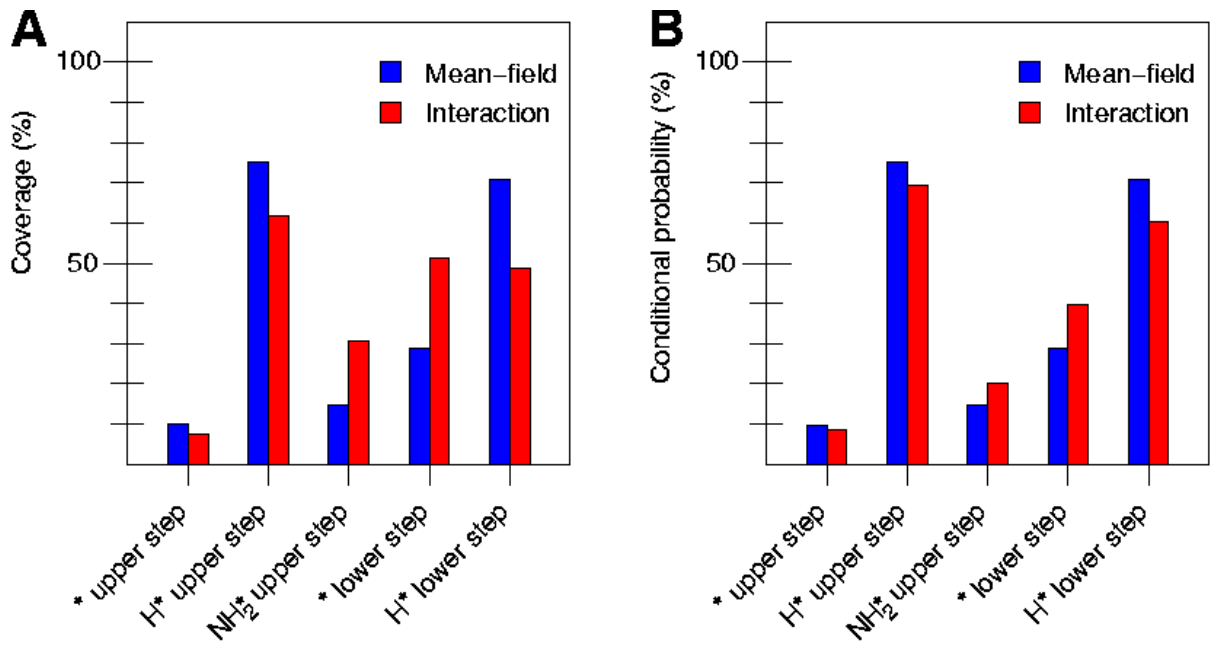


FIG 2

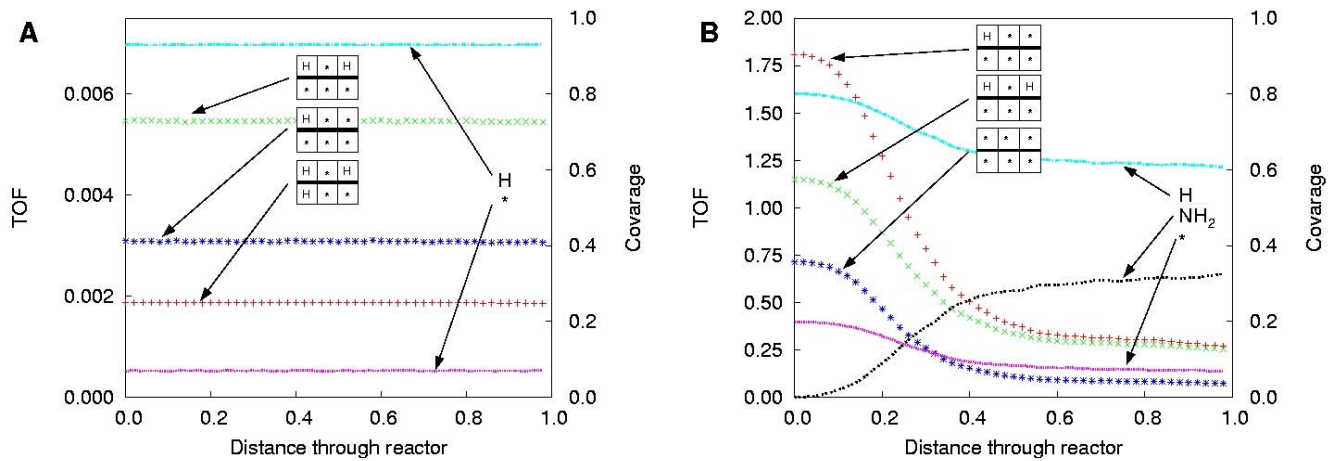


FIG 3

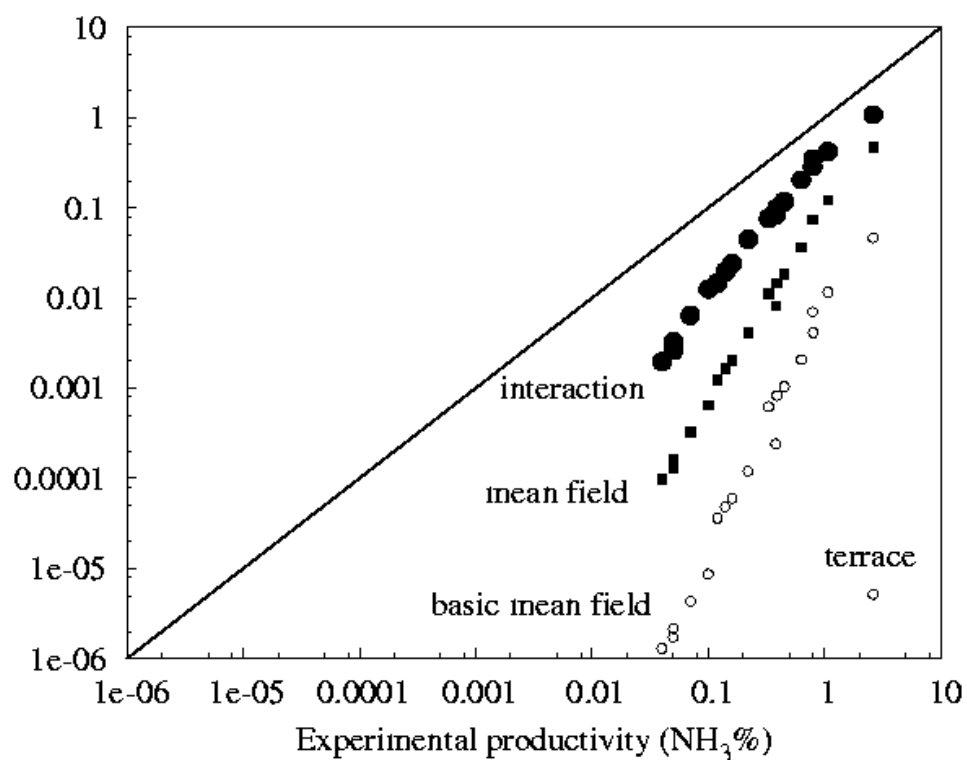


FIG 4

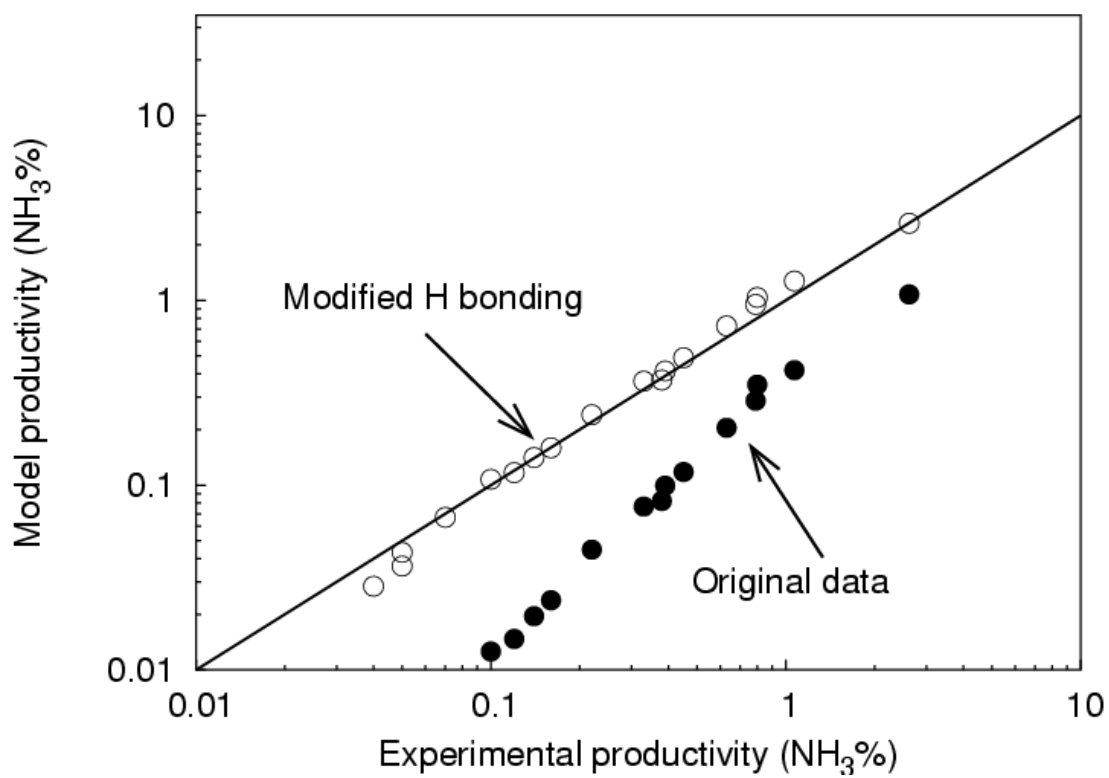


FIG 5

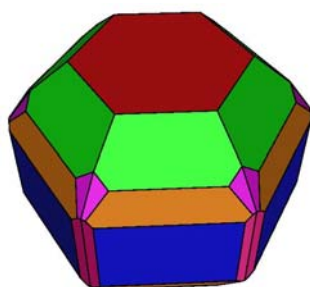


FIG 6

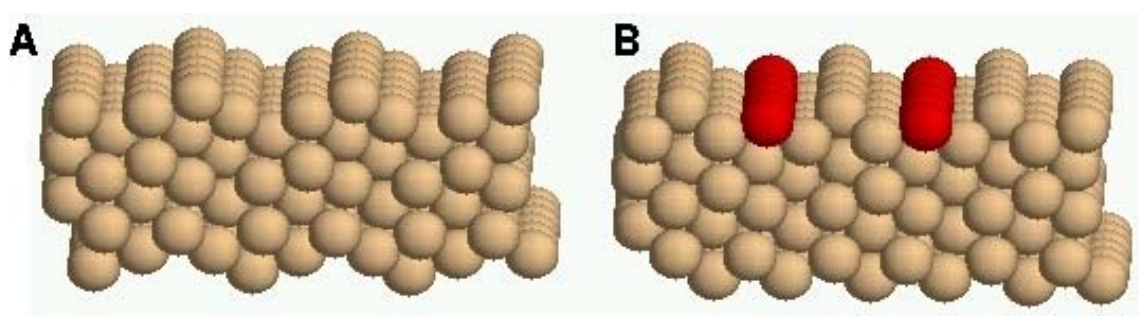


Fig. S1. (A) The coverage and (B) conditional probability for the different adsorbates calculated in the thermodynamic limit at $p_{H_2}=75$ bar, $p_{NH_3}=1$ bar, and $T=440$ °C. Here, results using the interactions given in Table S3 and using no interaction are shown.

Fig. S2. (A and B) The three main contributions to the rate depending on the different local environments and the coverages of different species on the upper step as we integrate through the reactor for two different temperatures, (A) $T=320$ °C and (B) $T=440$ °C. Here only the low flow 40 ml/min (STP) case is shown. A symbolic representation is used for the local environment showing in total four neighboring sites and two dissociation sites.

Fig. S3. Comparison of the experimentally measured (solid line) NH_3 productivity with three different theoretical models: basic mean field, mean field, and the interaction. The additional point (terrace) is the contribution from all of the terrace sites to the rate, calculated at high temperature 440 °C and low flow 40 ml/min (STP). It is concluded that even if roughly 60% of the all the sites on the Ru-particles

are terrace sites, compared to 2% that are B₅ sites, the high activation energy (1.9 eV) for the N₂ dissociation on the terrace make its contribution to the rate to be neglectable.

Fig. S4 Comparison of productivity calculated using original DFT energies (filled circles) and with modified H adsorption energy (open circles).

Fig. S5. Wulff construction for hcp Ru. The faces appearing in the construction are (001) (red), (100) (blue), (101) (green), (201) (orange), (111) (purple) and (210) (pink).

Fig. S6. Structures of Ru(103). Structure A (left) consists of a periodic arrangement of (100)/(101) edges, while structure B (right) consists of alternative A- and B-type steps. Structure B has a lower surface energy by 0.7 J/m², or 0.1 eV per removed edge atom.

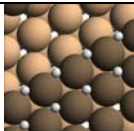
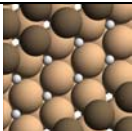
Tabel 1

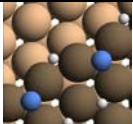
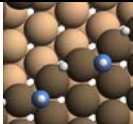
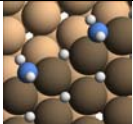
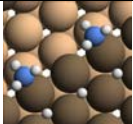
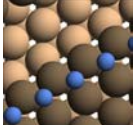
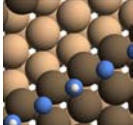
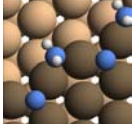
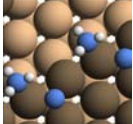
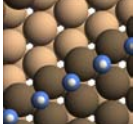
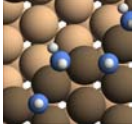
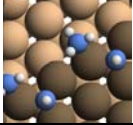
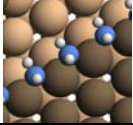
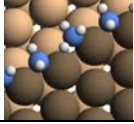
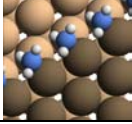
Species	Geometry	ΔE (eV/adsorbate)
H on the upper step	Bridge	-0.43
N	Hcp	-0.39
NH	Hcp	-1.01
NH ₂	Bridge	-1.74
NH ₃	On-top	-1.85
H on the lower step	Fcc	-0.36
N	Hcp	-0.16
NH	Hcp	-0.67
NH ₂	Fcc	-1.01
NH ₃	On-top	-1.46

Tabel 2

Species	Frequencies (meV)
H	44,123,161
N	53,57,68
NH	47,50,67,76,85,433
NH ₂	16,34,45,56,63,91,179,469,486
NH ₃	25,27,37,99,102,113,136,158,158,432,439,439
N ₂ at transition state	53,55,58,65,73

Tabel 3

E_{int} (eV)	Structure	E_{int} (eV)	Structure
0.024 H-H		0.06 H-H	

0.13 N-H		0.075 NH-H	
-0.05 NH ₂ -H		0.0 NH ₃ -H	
0.38 N-N		0.24 NH-N	
0.12 NH ₂ -N		-0.16 NH ₃ -N	
0.21 NH-NH		0.25 NH ₂ -NH	
0.18 NH ₃ -NH		0.43 NH ₂ -NH ₂	
0.30 NH ₃ -NH ₂		0.16 NH ₃ -NH ₃	

Tabel 4

(hkl)	E_{surf}	(hkl)	E_{surf}	(hkl)	E_{surf}
(001)	2.76	(100)A	3.07	(100)B	3.71
(110)	3.45	(101)A	3.15	(101)B	3.63
(111)A	3.39	(111)B	3.39	(102)A	3.25
(102)B	3.30	(201)A	3.51	(201)B	3.21
(210)A	3.41	(210)B	3.47		

Table S1. The optimal adsorption geometries and corresponding energies for all of the intermediates in the NH₃ synthesis reaction.

Table S2. The vibrational frequencies for the N₂ transition state and all of the intermediates.

Table S3. Interaction energies and geometries for different adsorbates on the upper and lower step.

Table S4. Surface energies (in J/m^2) for the considered Ru surfaces.

References:

1. B. Hammer, L. B. Hansen, J. K. Nørskov, *Phys. Rev. B* **59**, 7413 (1999).
2. D. Vanderbilt, *Phys. Rev. B* **41**, 7892 (1990).
3. A. Logadottir, J. K. Nørskov, *J. Catal.* **220**, 273 (2003).
4. D. P. Landau, K. Binder, *A Guide to Monte Carlo Simulations in Statistical Physics*, Cambridge University Press, Cambridge (2000).
5. K. Reuter, M. Scheffler, *Phys. Rev. Lett.* **90**, 046103 (2003) .
6. K. Reuter, M. Scheffler, *Phys. Rev. B* **68**, 045407 (2003) .
7. S. Dahl, J. Sehested, C. J. H. Jacobsen, E. Törnqvist, I. Chorkendorff, *J. Catal.* **192**, 391 (2000).